LETTER

doi:10.1038/nature12762

Puzzling accretion onto a black hole in the ultraluminous X-ray source M 101 ULX-1

Ji-Feng Liu[1], Joel N. Bregman[2], Yu Bai[1], Stephen Justham[1] & Paul Crowther [3]

There are two proposed explanations for ultraluminous X-ray sources[1,2] (ULXs) with luminosities in excess of 10^{39} erg s^{-1}. They could be intermediate-mass black holes (more than 100–1,000 solar masses, $M_{\odot}$) radiating at sub-maximal (sub-Eddington) rates, as in Galactic black-hole X-ray binaries but with larger, cooler accretion disks[3–5]. Alternatively, they could be stellar-mass black holes radiating at Eddington or super-Eddington rates[2,6]. On its discovery, M 101 ULX-1[4,7] had a luminosity of 3×10^{39} erg s^{-1} and a supersoft thermal disk spectrum with an exceptionally low temperature—uncomplicated by photons energized by a corona of hot electrons—more consistent with the expected appearance of an accreting intermediate-mass black hole[3,4]. Here we report optical spectroscopic monitoring of M 101 ULX-1. We confirm the previous suggestion[8] that the system contains a Wolf-Rayet star, and reveal that the orbital period is 8.2 days. The black hole has a minimum mass of $5M_{\odot}$, and more probably a mass of $20M_{\odot}-30M_{\odot}$, but we argue that it is very unlikely to be an intermediate-mass black hole. Therefore, its exceptionally soft spectra at high Eddington ratios violate the expectations for accretion onto stellar-mass black holes[9–11]. Accretion must occur from captured stellar wind, which has hitherto been thought to be so inefficient that it could not power an ultraluminous source[12,13].

Although it is desirable to obtain the primary mass of a ULX through measuring the motion of its companion (the secondary), this is only possible in the X-ray-low state (that is, at low X-ray luminosities) because the X-ray irradiated accretion disk will dominate optical emission in the X-ray-high state[14,15]. We performed a spectroscopic monitoring

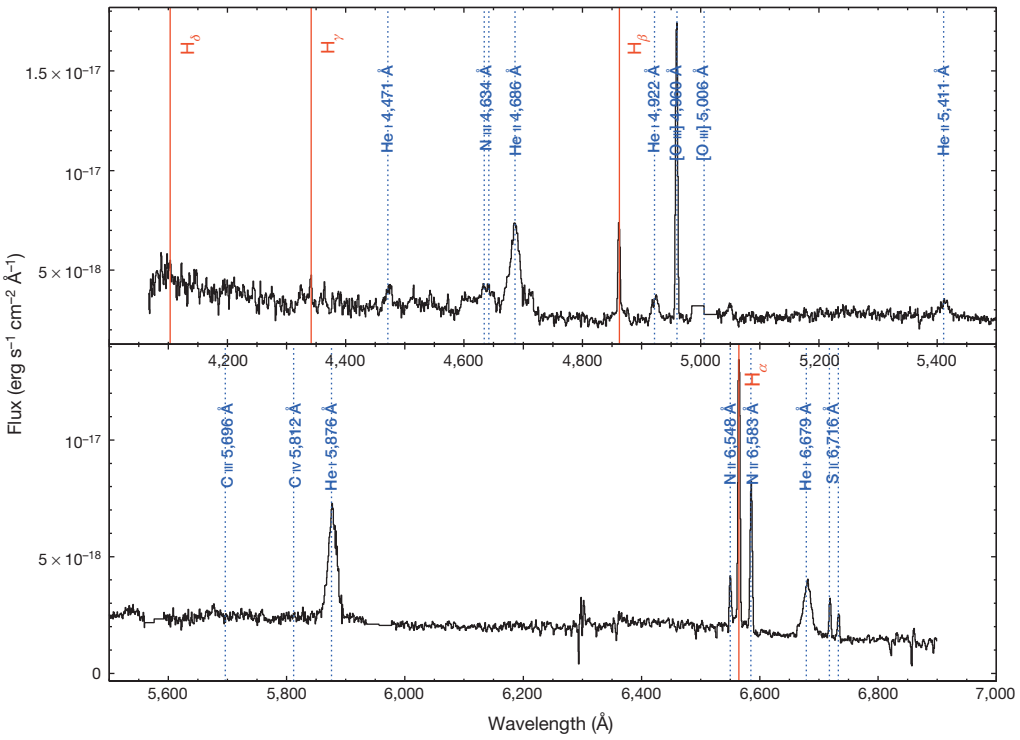

Figure 1 | The secondary of M 101 ULX-1 is confirmed to be a Wolf-Rayet star. Confirmation is based on the optical spectrum, combined from 10 Gemini/GMOS observations with a total exposure time of 16 h. The spectrum shows narrow nebular lines with a full-width at half-maximum (FWHM) of ~4 Å at the instrumental spectral resolution, including hydrogen Balmer lines and forbidden lines such as [O III] 4,960/5,006 Å (the latter is mostly in the CCD gap and only partly shown), [N II] 6,548/6,583 Å and [S II] 6,716/6,731 Å, all at a constant radial velocity over observations consistent with that of M 101. Also present are broad emission lines with FWHM up to 20 Å, including strong He II 4,686 Å, He I 5,876 Å and He I 6,679 Å lines, weaker He I 4,471 Å, He I 4,922 Å and He II 5,411 Å lines and N III 4,640 Å lines. The observed He I 5,876/He II 5,411 Å equivalent width ratio suggests a Wolf-Rayet star of WN8 sub-type, consistent with the absence of carbon emission lines for WC stars (such as C III 5,696 Å and C IV 5,812 Å). The intensities of the helium emission lines can be best reproduced by an atmospheric model[16] of a Wolf-Rayet star with $R_* = 10.7R_{\odot}$, $M_* = 17.5M_{\odot}$, $L_* = 5.4 \times 10^5 L_{\odot}$, $T_* = 48$ kK, $\dot{M}_* = 2 \pm 0.5 \times 10^{-5} M_{\odot}$ yr^{-1} and $v_{\infty} = 1{,}300 \pm 100$ km s^{-1} (with 68.3% uncertainties for the two continuously variable parameters; details of all parameters are given in Methods), consistent with those for a WN8 star. The mass–luminosity relation[17,18] for Wolf-Rayet stars gives a more reliable mass estimate of $19M_{\odot}$, which we use in the main text, with an estimated formal error of $1M_{\odot}$.

[1]Key Laboratory of Optical Astronomy, National Astronomical Observatories, Chinese Academy of Sciences, 20A Datun Road, Chaoyang District, 100012 Beijing, China. [2]Department of Astronomy, University of Michigan, 500 Church Street, Ann Arbor, Michigan 40185, USA. [3]Department of Physics and Astronomy, University of Sheffield, Hounsfield Road, Sheffield S3 7RH, UK.

campaign for M 101 ULX-1 from February to May 2010 during its expected X-ray-low states. The optical spectrum (Fig. 1) is characterized by broad helium emission lines, including the He II 4,686 Å line. Given the absence of broad hydrogen emission lines, which are detected in some ULXs from their X-ray irradiated accretion disk at very high luminosities[14,15], the donor cannot be hydrogen rich, and thus must be a Wolf-Rayet star or a helium white dwarf. The latter can be excluded because a white dwarf is roughly a million times dimmer than the observed optical counterpart even during the low states. Indeed, the optical spectrum is unique to Wolf-Rayet stars, and the intensities of the helium emission lines can be reproduced well by an atmospheric model[16] of such a star, the mass of which is estimated to be $19M_{\odot}$ on the basis of the empirical mass–luminosity relation[17,18]. Given the relatively low luminosities in the X-ray-low state, the helium emission lines are expected to originate mainly from the Wolf-Rayet secondary with little contribution from the accretion disk. Such emission lines have been used to measure the black-hole mass in both IC 10 X-1 ($21M_{\odot}$–$35M_{\odot}$)[19,20] and NGC 300 X-1 ($12M_{\odot}$–$24M_{\odot}$)[21,22], systems that exhibit luminosities an order of magnitude lower than the peak luminosity of M 101 ULX-1.

Because the centroid of the He II 4,686 Å emission line varied by $\pm 60\ \mathrm{km\ s^{-1}}$ over the three months of our monitoring campaign, we have been able to obtain the orbital period of $P = 8.2 \pm 0.1$ days and the mass function $f(M_*, M_\bullet, i) = 0.18M_{\odot} \pm 0.03M_{\odot}$ for M 101 ULX-1 (Fig. 2). Because we already know the mass of the donor star (M_*) we are able to infer the mass of the accretor to be $M_\bullet \geq 4.6M_{\odot} \pm 0.3M_{\odot}$ (for inclination angle $i \leq 90^{\circ}$), where the error is computed from the uncertainties in the secondary mass and in the mass function. Even for the minimum mass, obtained when the system is aligned perfectly edge-on to the line of sight (for which $i = 90^{\circ}$), such a compact primary can only be a black hole. Higher black-hole masses are easily obtained for lower inclination angles. For example, a stellar-mass black hole of $20M_{\odot}$ corresponds to $i = 19^{\circ}$, and an intermediate-mass black hole (IMBH) of $1{,}000M_{\odot}$ ($300M_{\odot}$) corresponds to $i = 3^{\circ}$ ($i = 5^{\circ}$). The probability of discovering a pole-on binary with $i < 3^{\circ}$ ($i = 5^{\circ}$) by mere chance is lower than 0.1% (0.3%). This makes it very unlikely that this system contains an IMBH of $1{,}000M_{\odot}$ ($300M_{\odot}$). If the peak luminosity of M 101 ULX-1 corresponds to less than 30% of the Eddington level—which is commonly assumed to be required to produce the thermally dominated spectral state[9,23]—then the black-hole mass would exceed $50M_{\odot}$–$80M_{\odot}$. The true black-hole mass seems likely to be $\sim 20M_{\odot}$–$30M_{\odot}$ (see Methods for details).

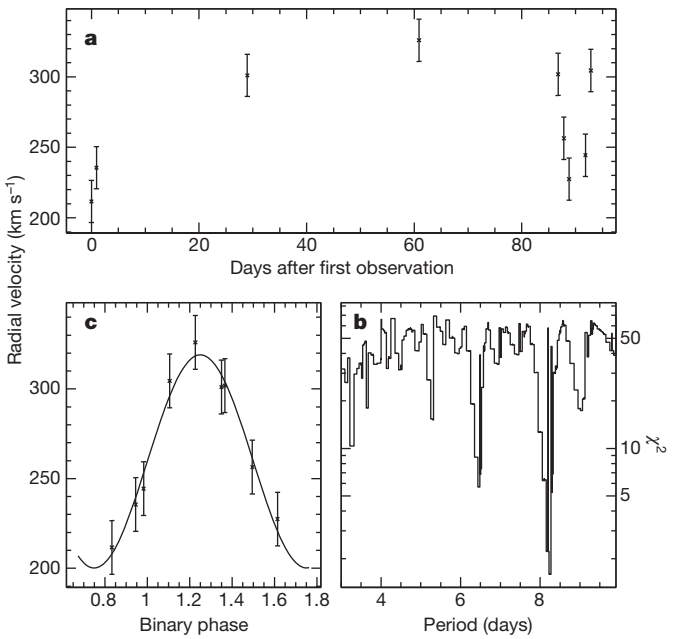

Figure 2 | An orbital period of ~8.2 days is revealed by radial velocity measurements taken over three months for M 101 ULX-1. a, Radial velocities of the He II 4,686 Å emission line (with 68.3% uncertainties computed mainly from the dispersion of the wavelength calibration) from nine observations over three months. **b**, **c**, χ^2 computed for a sine fit (under the assumption of a circular orbit) to the radial velocity curve as a function of trial periods (**b**). The trial periods range from a minimum of 3 days, when the Wolf-Rayet secondary fills its Roche lobe, to a maximum of 10 days as suggested by the last five measurements. The best fit is achieved at minimal $\chi^2 \approx 1.6$ for $P = 8.2$ days and $K = 61\ \mathrm{km\ s^{-1}}$, for which the folded radial velocity curve is shown in **c**. The 68.3% uncertainties for the best fit are estimated to be $\Delta P = 0.1$ days and $\Delta K = 5\ \mathrm{km\ s^{-1}}$ using $\chi^2 - \chi^2_{\mathrm{best}} = 1$. All other trial periods (such as those at $P \approx 6.4$ days) are worse by $\Delta\chi^2 > 4$. The successful fit with a sine curve suggests that the orbital eccentricity is small. This leads to a mass function $f(M_*, M_\bullet, i) = \dfrac{PK^3}{2\pi G} = 0.18M_{\odot} \pm 0.03M_{\odot}$, where the error accounts for the 68.3% uncertainties in P and K.

The confirmation of a Wolf-Rayet star in the system, independent of the dynamical mass measurement, also suggests that M 101 ULX-1 is unlikely to be an IMBH. IMBHs cannot form directly through the collapse of massive stars, but it is suggested that they can form through mergers in dense stellar environments[24,25]. However, any IMBH formed would not be seen as a ULX unless they capture a companion as a reservoir from which to accrete matter. Such a capture is a rare event even in dense stellar environments such as globular clusters or galactic bulges, to which M 101 ULX-1 apparently does not belong, and captures that can provide high-enough accretion rates to power a ULX are even more unusual[26,27]. Given the rarity of Wolf-Rayet stars (there are about 2,000 such stars out of the 200 billion stars in a typical spiral galaxy like the Milky Way[18]), it is extremely unlikely that M 101 ULX-1 is such a revived IMBH. Alternatively a huge population of IMBHs could somehow remain undetected, both with and without companions.

M 101 ULX-1 is thus a stellar black hole, although it is a member of the class of supersoft ULXs which have been considered to be outstanding IMBH candidates[4,5]. Its combination of high luminosities and low disk temperatures (Fig. 3) strains our current understanding of accretion by stellar-mass black holes[9–11]. Studies of Galactic black-hole X-ray binaries suggest that radiation at less than roughly 30% of the Eddington luminosity is dominated by the thermal emission from a hot disk (~1 keV). A hard power-law component due to Comptonization by the disk corona becomes more and more significant when the luminosity increases to near-Eddington levels. When the luminosity increases further, to Eddington or super-Eddington levels, the Comptonized component begins to dominate the disk component, as observed for ULXs in the ultraluminous state[2,6]. For example, the ultraluminous microquasar in M31 with a stellar-mass black hole ($\sim 10M_{\odot}$) and a luminosity of $10^{39}\ \mathrm{erg\ s^{-1}}$ exhibited hard X-ray spectra[28]. If it were the same phenomenon, a hard X-ray spectrum would be expected for a stellar-mass black hole in M 101 ULX-1, whether it is radiating at sub-, near- or super-Eddington luminosities. The observed supersoft X-ray spectra lack hard photons above 1.5 keV, and can be described purely by cool accretion disks, uncomplicated by Comptonization, with exceptionally low temperatures of 90–180 eV (refs 4, 7). Including extra photoelectric absorption by the surrounding Wolf-Rayet wind in the spectral analysis would further lower the underlying disk temperatures and increase the luminosities[4], which would cause M 101 ULX-1 to deviate even farther from the expected hard spectra. This unambiguously demonstrates that stellar-mass black holes can have very cool accretion disks uncomplicated by the Comptonized component, contrary to standard expectations[3,9,11].

M 101 ULX-1 is the third known Wolf-Rayet/black-hole binary but is distinctly different from NGC 300 X-1 and IC 10 X-1. Whereas M 101 ULX-1 is a recurrent transient with supersoft spectra and low disk temperatures, both IC 10 X-1 and NGC 300 X-1 show constant X-ray output (despite apparent variations due to orbital modulation), hard spectra with a minor disk component, and disk temperatures above 1 keV (refs 19, 21, 29; Fig. 3). Hence the compact object in M 101 ULX-1 was considered to be an excellent IMBH candidate, whereas IC 10 X-1

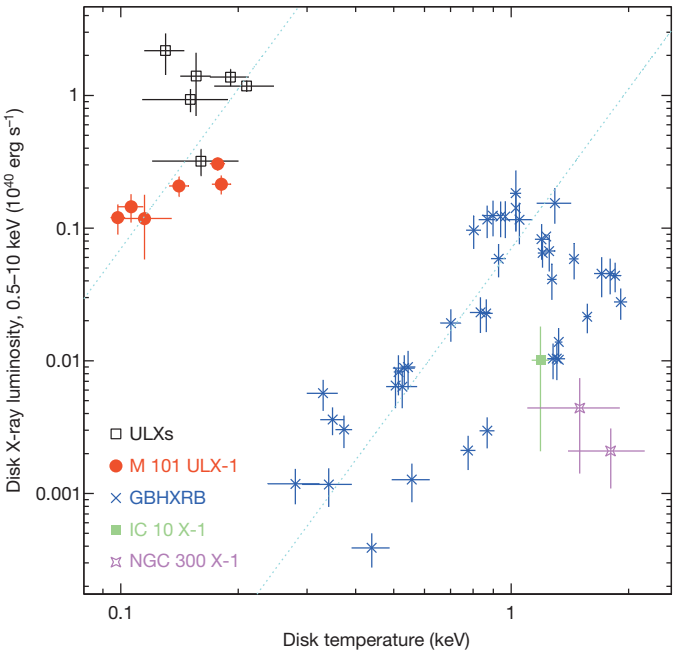

Figure 3 | The prototype ultraluminous supersoft X-ray source M 101 ULX-1 exhibits distinct spectral characteristics. M 101 ULX-1 is compared to Galactic black-hole X-ray binaries (GBHXRBs), Wolf-Rayet/black hole binaries IC 10 X-1 and NGC 300 X-1, and other ULXs on the disk X-ray luminosity (L_X) versus disk temperature (T_d) plane, all plotted with the 68.3% uncertainties from the X-ray spectral fitting. Except for M 101 ULX-1, which can be fitted with a disk blackbody model with temperatures of 90–180 eV (refs 4, 7), all other X-ray sources are complicated by the presence of a hard power-law component due to Comptonization by a corona, and can be best fitted with a disk blackbody plus power-law composite model[3,29]. Whereas GBHXRBs[3] and the other two Wolf-Rayet/black-hole binaries[29] with stellar black holes cluster in the same region, M 101 ULX-1 lies within a distinct region that has been expected to contain IMBH candidates, the same region as for some ULXs[3]. The dotted lines describe the expected disk luminosity (L_d) for different disk temperatures for a fixed disk inner radius (R_{in}) based on the relation $L_d \propto R_{in}^2 T_d^4$. The two lines are offset by four orders of magnitude in luminosity, implying a factor of 100 differences in the disk inner radii, and a factor of 100 differences in the black-hole masses if the disk radius is tied to the innermost stable orbit of the black hole. Fitting ULX spectra with alternative Comptonization models can yield high disk temperatures consistent with those of stellar-mass black holes[6]. However, the location of M 101 ULX-1 on the L_X–T_d plane does not change because its spectra are not complicated by Comptonization.

and NGC 300 X-1 were expected to host stellar-mass black holes (as was later confirmed). The 8.2-day orbital period shows that M 101 ULX-1 is a wide binary, with components that would be separated by $50R_\odot$ for black-hole mass $M_\bullet = 5M_\odot$ ($75R_\odot$ for $M_\bullet = 60M_\odot$). The Roche lobe radius for the secondary is always greater than $22R_\odot$, twice as large as the Wolf-Rayet star itself. Mass transfer by Roche lobe overflow is thus impossible, and the black hole must be accreting matter by capturing the thick stellar wind. Given the geometry of the system, the disk is very large, and thus there will be a helium partial ionization zone. Such a disk is prone to instability, causing the observed X-ray transient behaviours for M 101 ULX-1. In contrast, IC 10 X-1 and NGC 300 X-1 have shorter orbital periods (34.9 h and 32.3 h respectively) and smaller separations ($\sim 20R_\odot$). Because those Wolf-Rayet stars fill their Roche lobes, the black holes accrete via Roche-lobe overflow. These systems also have much smaller and hotter accretion disks without helium partial ionization zones, which explains why IC 10 X-1 and NGC 300 X-1 do not display disk-instability outbursts (see also Methods).

Mass transfer through wind accretion usually has a very low efficiency, as in the case of many low-luminosity, high-mass X-ray binaries, and is typically not considered for populations that require high accretion rates. However, M 101 ULX-1 demonstrates that this expectation is not always correct. In particular, transient outbursts of such wind-accreting system have generally not been included in theoretical ULX populations[12,13], but M 101 ULX-1 does attain ULX luminosities. Theorists have recently suggested that wind accretion may potentially also be significant for some progenitors of type Ia supernovae[30]. M 101 ULX-1 empirically supports this reassessment of the potential importance of wind accretion.

METHODS SUMMARY

Analysis of earlier M 101 ULX-1 observations, data reduction and analysis of the Gemini/GMOS spectroscopic observations, determination of the Wolf-Rayet subclass and its physical parameters, the search for orbital periodicity, and determination of the properties of the Wolf-Rayet/black-hole binary are described in Methods.

Online Content Any additional Methods, Extended Data display items and Source Data are available in the online version of the paper; references unique to these sections appear only in the online paper.

Received 1 April; accepted 27 September 2013.

1. Fabbiano, G. The hunt for intermediate-mass black holes. *Science* **307,** 533–534 (2005).
2. Gladstone, J. The sub-classes of ultraluminous X-ray sources. Preprint at http://arXiv.org/abs/1306.6886 (2013).
3. Miller, J. *et al.* A comparison of intermediate mass black hole candidate ultraluminous X-ray sources and stellar mass black holes. *Astrophys. J.* **614,** L117–L120 (2004).
4. Kong, A. K. H., Di Stefano, R. & Yuan, F. Evidence of an intermediate-mass black hole: Chandra and XMM-Newton observations of the ultraluminous supersoft X-ray source in M101 during its 2004 outburst. *Astrophys. J.* **617,** L49–L52 (2004).
5. Liu, J. F. & Di Stefano, R. An ultraluminous supersoft X-ray source in M81: an intermediate-mass black hole? *Astrophys. J.* **674,** L73–L77 (2008).
6. Gladstone, J. *et al.* The ultraluminous state. *Mon. Not. R. Astron. Soc.* **397,** 1836–1851 (2009).
7. Mukai, K., Still, M., Corbet, R., Kuntz, K. & Barnard, R. The X-ray properties of M101 ULX-1 = CXOKM101 J140332.74+542102. *Astrophys. J.* **634,** 1085–1092 (2005).
8. Liu, J. F. Multi-epoch multi-wavelength study of an ultraluminous X-ray source in M101: the nature of the secondary. *Astrophys. J.* **704,** 1628–1639 (2009).
9. McClintock, J. & Remillard, R. in *Compact Stellar X-ray Sources* (eds Lewin, W. & van der Klis, M.) 157–213 (Cambridge Astrophysics Series No. 39, Cambridge Univ. Press, 2006).
10. Esin, A. A., McClintock, J. E. & Narayan, R. Advection-dominated accretion and the spectral states of black hole X-ray binaries: application to nova Muscae 1991. *Astrophys. J.* **489,** 865–889 (1997).
11. Remillard, R. A. & McClintock, J. E. X-ray properties of black-hole binaries. *Annu. Rev. Astron. Astrophys.* **44,** 49–92 (2006).
12. Rappaport, S., Podsiadlowski, Ph. & Pfahl, E. Stellar-mass black hole binaries as ultraluminous X-ray sources. *Mon. Not. R. Astron. Soc.* **356,** 401–414 (2005).
13. Linden, T. *et al.* The effect of starburst metallicity on bright X-ray binary formation pathways. *Astrophys. J.* **725,** 1984–1994 (2010).
14. Roberts, T. P. *et al.* (No) dynamical constraints on the mass of the black hole in two ULXs. *Astron. Nachr.* **332,** 398–401 (2011).
15. Cseh, D., Gris'e, F., Corbel, S. & Kaaret, P. Broad components in optical emission lines from the ultraluminous X-ray source NGC 5408 X-1. *Astrophys. J.* **728,** L5–L9 (2011).
16. Hillier, D. J. & Miller, D. L. The treatment of non-LTE line blanketing in spherically expanding outflows. *Astrophys. J.* **496,** 407–427 (1998).
17. Schaerer, D. & Maeder, A. Basic relations between physical parameters of Wolf-Rayet stars. *Astron. Astrophys.* **263,** 129–136 (1992).
18. Crowther, P. A. Physical properties of Wolf-Rayet stars. *Annu. Rev. Astron. Astrophys.* **45,** 177–219 (2007).
19. Prestwich, A. H. *et al.* The orbital period of the Wolf-Rayet binary IC 10 X-1: dynamic evidence that the compact object is a black hole. *Astrophys. J.* **669,** L21–L24 (2007).
20. Silverman, J. M. & Filippenko, A. V. On IC 10 X-1, the most massive known stellar-mass black hole. *Astrophys. J.* **678,** L17–L20 (2008).
21. Carpano, S. *et al.* A 33 hour period for the Wolf-Rayet/black hole X-ray binary candidate NGC 300 X-1. *Astron. Astrophys.* **466,** L17–L20 (2007).
22. Crowther, P. A. *et al.* NGC 300 X-1 is a Wolf-Rayet/black hole binary. *Mon. Not. R. Astron. Soc.* **403,** L41–L45 (2010).
23. Steiner, J. F., McClintock, J. E., Remillard, R. A., Narayan, R. & Gou, L. J. Measuring black hole spin via the X-ray continuum-fitting method: beyond the thermal dominant state. *Astrophys. J.* **701,** L83–L86 (2009).
24. Miller, M. C. & Hamilton, D. P. Production of intermediate-mass black holes in globular clusters. *Mon. Not. R. Astron. Soc.* **330,** 232–240 (2002).
25. Portegies Zwart, S. F., Baumgardt, H., Hut, P., Makino, J. & McMillan, S. L. W. Formation of massive black holes through runaway collisions in dense young star clusters. *Nature* **428,** 724–726 (2004).
26. Blecha, L. *et al.* Close binary interactions of intermediate-mass black holes: possible ultra-luminous X-ray sources? *Astrophys. J.* **642,** 427–437 (2006).

27. Madhusudhan, N. *et al.* Models of ultraluminous X-ray sources with intermediate-mass black holes. *Astrophys. J.* **640,** 918–922 (2006).
28. Middleton, M. J. *et al.* Bright radio emission from an ultraluminous stellar-mass microquasar in M31. *Nature* **493,** 187–190 (2013).
29. Barnard, R., Clark, J. S. & Kolb, U. C. NGC 300 X-1 and IC 10 X-1: a new breed of black hole binary? *Astron. Astrophys.* **488,** 697–703 (2008).
30. Mohamed, S. & Podsiadlowski, Ph. Mass transfer in Mira-type binaries. *Balt. Astron.* **21,** 88–96 (2011).

Acknowledgements We thank J. McClintock, R. Di Stefano, Q.-Z. Liu, X.-D. Li, F. Yuan and S.-N. Zhang for discussions. J.-F.L. acknowledges support for this work provided by NASA through the Chandra Fellowship Program (grant PF6-70043), support from the Chinese Academy of Sciences through grant KJCX2-EW-T01 and support by the National Science Foundation of China through grants NSFC-11273028 and NSFC-11333004. The paper is based on observations obtained at the Gemini Observatory, which is operated by the Association of Universities for Research in Astronomy, Inc., under a cooperative agreement with the NSF on behalf of the Gemini partnership: the National Science Foundation (United States), the National Research Council (Canada), CONICYT (Chile), the Australian Research Council (Australia), Ministério da Ciência, Tecnologia e Inovação (Brazil) and Ministerio de Ciencia, Tecnología e Innovación Productiva (Argentina).

Author Contributions J.-F.L. and J.N.B. proposed the observations, J.-F.L. and Y.B. reduced the data and carried out the analysis, J.-F.L., J.N.B. and S.J. discussed the results and wrote the paper, and P.C. helped to confirm the properties of the Wolf-Rayet star. All authors commented on the manuscript and contributed to the revision of the manuscript.

Author Information Reprints and permissions information is available at www.nature.com/reprints. The authors declare no competing financial interests. Readers are welcome to comment on the online version of the paper. Correspondence and requests for materials should be addressed to J.-F.L. (jfliu@nao.cas.cn).

METHODS

Analysis of earlier M 101 ULX-1 observations. M 101 is a nearby face-on grand design spiral galaxy, a frequent target of various observations. These include the optical monitoring observations in search of Cepheids with the Hubble Space Telescope, yielding a distance of 6.855 Mpc (ref. 31). M 101 ULX-1 (CXO J140332.3+542103) is located near a spiral arm (Extended Data Fig. 1), and identified with a unique optical counterpart of $V = 23.5$ mag (ref. 32). At this location, the metallicity is 0.4 times solar according to the M 101 gas-phase oxygen abundance gradient[33].

This ULX has been observed intensively by X-ray missions including ROSAT, XMM and Chandra since early 1990s, which exhibited spectral state transitions between the low-hard state and the high-soft state reminiscent of Galactic black-hole X-ray binaries. This ULX was once the brightest X-ray point source in M 101 with a Chandra/ACIS count rate of 0.10 counts s^{-1} (ref. 34), observed during the 2000 March observation (ObsID 934). The Chandra/XMM-Newton spectra during its outbursts[4,35] were very soft and can be generally fitted with an absorbed blackbody model with neutral hydrogen column density $n_H = (1–4) \times 10^{21}$ cm^{-2} and temperatures of 50–100 eV, and the peak 0.3–7 keV luminosity reached 3×10^{40} erg s^{-1}, with a bolometric luminosity of about 10^{41} erg s^{-1}, suggesting an IMBH of a few thousand solar masses. It was argued that it is unphysical to adopt a high neutral hydrogen column density of $\geq 10^{21}$ cm^{-2}, and fitting the spectra as blackbody plus a diskline component centred at 0.5 keV with n_H fixed at the Galactic value of 4×10^{20} cm^{-2} yielded the maximum outburst bolometric luminosity of 3×10^{39} erg s^{-1}, consistent with the Eddington luminosity of a black hole of $20M_\odot$–$40M_\odot$ (ref. 7).

Even at the lowered luminosities of 3×10^{39} erg s^{-1}, the combination of the disk luminosities and disk temperatures makes M 101 ULX-1 an outstanding IMBH candidate. It is believed that the accretion disks for IMBHs should have larger inner radii and consequently lower disk temperatures[3–5], occupying the upper left portion in the T_d–L_X plane as shown in Fig. 3. The position of M 101 ULX-1 on this plane suggests that it is distinctly different from the Galactic black-hole X-ray binaries in the lower right portion, but belongs to the league of IMBH candidates along with some extreme ULXs above 10^{40} erg s^{-1}. The practice of placing these ULXs on this plane was questioned because decomposing ULX spectra into disk blackbody plus power-law models is unphysical given the dominance of the hard power-law component. However, in the case of M 101 ULX-1 the spectra are supersoft without any hard power-law component, so its location on the plane should reflect the accretion disk uncomplicated by Comptonization. For comparison, we also put on this plane the other two known Wolf-Rayet/black-hole binaries[29] IC 10 X-1 and NGC 300 X-1, which apparently belong to the league of stellar-mass black holes, and dynamical mass measurements have yielded mass estimates of $20M_\odot$–$30M_\odot$.

Combined analysis of 26 HST observations and 33 X-ray observations over 16 years[8] revealed two optical outbursts in addition to 5 X-ray outbursts. Although there is no 'exact' period for the recurring outbursts, the outbursts occur once roughly every six months. Such outbursts last 10–30 days, suggesting an outburst duty cycle of 10–15%. Outside outbursts, ULX-1 stays in a low-hard state with an X-ray luminosity of 2×10^{37} erg s^{-1} (refs 4, 7, 8, 35). Such behaviour is reminiscent of those of soft X-ray transients in low-mass X-ray binaries, albeit with higher luminosities and lower disk temperatures, but is different from the recently discovered high-mass fast transients owing to clumping winds at much lower X-ray luminosities ($\sim 10^{34}$ erg s^{-1}). Detailed studies of the optical spectral energy distribution, after removal of optical emission from the X-ray irradiated accretion disk in the outbursts, suggest that the secondary is a Wolf-Rayet star of initially $40M_\odot$–$60M_\odot$, currently $18M_\odot$–$20M_\odot$, $9R_\odot$–$12R_\odot$ and about 5×10^4 K (ref. 8). This claim of a Wolf-Rayet companion is supported by the presence of the He II 4,686 Å emission line in the Gemini/GMOS-N spectrum taken in 2005[36].

Gemini/GMOS data reduction. M 101 ULX-1 was monitored spectroscopically from February to May in 2010 during its expected low states under the Gemini/GMOS-N program GN-2010A-Q49 (PI: J.-F.L.). Extended Data Table 1 lists the observations taken in ten nights distributed from February to May, with a total exposure of 15.6 h. All exposures were taken with the 0.75″ slit and the B600 grating tuned for a wavelength coverage from 4,000–6,900 Å; such a slit/grating combination will yield a spectral resolution of about 4.5 Å. We followed standard procedures to reduce the observations and extract 1D spectra using the gmos package in IRAF. All consecutive sub-exposures during one night were combined into one spectrum to increase the signal-to-noise ratio, and we obtained ten spectra with exposure times ranging from 3,200 s to 9,600 s (Extended Data Table 1).

For each spectrum, the wavelength solution was obtained using the copper–argon arc lamp spectra taken with the same slit/grating setting right before and after the science exposures during the same night or occasionally the night after. We verified the wavelength solution by comparing thus-obtained wavelengths to the intrinsic wavelengths for a dozen of strong night sky emission lines identified in the spectra before sky subtraction, and revealed wavelength differences with a dispersion of about 0.25 Å or $\sim$15 km s^{-1}. The extracted spectra were converted to flux spectra using the standard star HZ44 taken during the night of February 15, and we scaled the spectra to have specific flux $f_\lambda = 1.5 \times 10^{-18}$ erg s^{-1} cm^{-2} $Å^{-1}$ at 5,500 Å corresponding to F555W = 23.5 mag based on previous HST/WFPC2 observations[8].

Figure 1 shows the flux-calibrated sky-subtracted spectrum combined from the ten spectra. The combined spectrum is free of absorption lines but abundant in emission lines as identified and listed in Extended Data Table 2. For each emission line, we fit a Gaussian profile to derive its line width and compute its line flux and luminosity. Two categories of lines are present in the spectrum. The first category is the broad helium emission lines with FWHM of up to 20 Å, five times broader than the instrumental spectral resolution, and includes strong He II 4,686 Å, He I 5,876 Å, He I 6,679 Å, and weaker He I 4,471 Å, He I 4,922 Å, and He II 5,411 Å lines. The broad N III 4,634 Å emission line is also present. The second category is the narrow emission lines with line widths consistent with the instrumental spectral resolution, and includes the Balmer lines and forbidden lines such as [O III] 4,960/5,006 Å (the latter is mostly in the CCD gap and not listed), [N II] 6,548/6,583 Å, and [S II] 6,716/6,731 Å.

The emission line properties are derived from the Gaussian line profile fitting. The average line properties including FWHM, equivalent width, and line luminosities are measured from the combined spectrum (Extended Data Table 2). The shifts of the line centres were also measured for individual spectra, with the barycentric correction computed using the rvsao package in IRAF as listed in Extended Data Table 1 for each spectrum. It was found that the line shifts, after barycentric correction, are consistent with being constant for narrow emission lines over all observations at 230 ± 15 km s^{-1}, consistent with the radial velocity of 241 ± 2 km s^{-1} for the face-on M 101. However, the broad helium emission lines, as measured with the strongest He II 4,686 Å line, shifted from observation to observation between 210 km s^{-1} and 330 km s^{-1} as listed in Extended Data Table 1, with an average of 270 km s^{-1} that is significantly different from that for nebular lines.

The properties of the nebular lines help to determine the environmental metallicity and the neutral hydrogen column density. The line intensity ratio between [N II] 6,583 Å and H_α, $N2 \equiv$ [N II]λ6,583/H_α, can be used as an abundance indicator[37] with $12 + \log(O/H) = 8.90 + 0.57 \times N2$, albeit with a large dispersion in log(O/H) of ±0.41. Given the equivalent width of these two lines (Extended Data Table 2), we find $12 + \log(O/H) = 8.70$, close to solar metallicity (8.66). This is higher than but marginally consistent with the value of 0.4 times solar according to the M 101 gas-phase oxygen abundance gradient[33] given the location of ULX-1. The observed Balmer line flux ratios can be used to infer the dust extinction between the nebula and the observer. In the nebular emission around ULX-1, the intrinsic ratio H_α/H_β is 2.74 in case B for a thermal temperature of $T = 20{,}000$ K (ref. 38). Assuming $E(B-V) = 0.1$ mag, then $A_{6564} = 0.250$ mag, $A_{4863} = 0.360$ mag, $\Delta A = 0.11$ mag, $\Delta H_\alpha/\Delta H_\beta = 1.1$, and reddened $H_\alpha/H_\beta \approx 3$. The observed H_α/H_β is 2.85, suggesting that the extinction is low, and using the Galactic value is reasonable.

Determining the Wolf-Rayet subclass of binary ULX-1. The broad helium emission lines in the newly obtained Gemini/GMOS spectrum are typical of an extremely hot, hydrogen-depleted Wolf-Rayet star. Accretion disks around a compact object can also give rise to broad helium emission lines, but a broad Balmer line is expected to be present and much stronger than the helium lines. Indeed, broad H_β emission lines are present in two ULXs with optical spectra (4,000–5,400 Å), NGC1313 X-2[14] and NGC 5408 X-1[15], and are stronger than the He II 4,686 Å emission line. In the ULX-1 spectrum (Fig. 1), although the Balmer emission lines are present, they are narrow emission lines like forbidden lines, and should come from the surrounding nebulae, as evidenced by their nearly constant line shifts from observation to observation, in distinct contrast to helium lines with line shift differences of ±60 km s^{-1}.

The sub-type of this Wolf-Rayet star can be determined from the presence or absence of line species in the spectrum[18]. There are two main types of Wolf-Rayet stars, WN stars with $R \approx 5R_\odot$–$12R_\odot$ revealing H-burning products, and subsequently more compact WC stars with $R \approx 2R_\odot$–$3R_\odot$ revealing He-burning products. Spectra of WC stars are dominated by carbon lines (such as C III 4,650 Å, C III 5,696 Å and C IV 5,812 Å) that are stronger than helium lines, but none of the carbon lines are present in the ULX-1 spectrum. WN stars from WN4 to WN8 show[39] increasing absolute magnitudes M_V from −3.5 mag to −6 mag, increasing mass loss rates from $10^{-5}M_\odot$ yr^{-1} to $10^{-4}M_\odot$ yr^{-1}, decreasing effective temperatures from 80 kK to 45 kK, and hence an increasing fraction of He I atoms relative to He II ions. Comparing the observed spectrum to the spectral atlas of WN stars[18,40], we estimate a late-type WN8 star. A WN8 subtype is also inferred based on the He I 5,876 Å /He I 5,411 Å equivalent width ratio[41]. Such a subtype is roughly consistent with its absolute magnitude of $M_V = -5.9$ mag (after extinction correction using Galactic $E(B-V) = 0.1$ mag and $R_V = 3.1$), and the effective temperature of about 50 kK derived from its broad-band spectral energy distribution[8].

Determining physical parameters for the Wolf-Rayet star. As for the case of NGC 300 X-1[22], we have calculated synthetic models using the line-blanketed,

non-local thermodynamic equilibrium model atmosphere code[16]. To select the best physical parameters of the Wolf-Rayet star, we compare the model equivalent width EW with observed values for the six helium emission lines and minimize the quantity $\Delta^2 = \Sigma_i(\mathrm{EW} - \mathrm{EW}_i)^2$. In all model calculations, elemental abundances are set to 40% of the solar value for the metallicity of $0.4Z_\odot$ at the location of ULX-1. We vary the stellar radius R_* between $4R_\odot$ and $20R_\odot$, stellar mass M_* between $5M_\odot$ and $35M_\odot$, stellar luminosity L_* in the range $(5\text{–}100)\times10^4L_\odot$, the outer radius for the line-forming region R_{MAX} up to $40R_\odot$, the terminal velocity v_∞ between 400 and 2,000 km s^{-1}, and the stellar wind mass loss rate $\dot{M}_*$ in the range $(5\text{–}100)\times10^{-6}M_\odot\,\mathrm{yr}^{-1}$.

We have run ~5,000 models with the combinations of stellar mass, radius and luminosity determined by the stellar evolution tracks[42] of $Z = 0.4Z_\odot$ for all possible WN stars, and another ~5,000 models with 'fake' stars whose mass, radius and luminosity are completely independent of each other. After a total of ~10,000 model evaluations, a best-fitting model is found with $R_* = 10.7R_\odot$, $M_* = 17.5M_\odot$, $L_* = 5.4\times10^5L_\odot$, $v_\infty = 1{,}300$ km s^{-1}, $R_{\mathrm{MAX}} = 22R_\odot$ and $\dot{M}_* = 2.0\times10^{-5}M_\odot\,\mathrm{yr}^{-1}$. The model reproduces the helium emission lines extremely well (Extended Data Table 2), with an average difference of $|\Delta| = 0.6$ Å. In comparison, the majority of models and all models with 'fake' stellar parameters are much worse-fitting with $\Delta^2 \gg 10$ (Extended Data Fig. 2). Based on the Δ^2 distribution, our model evaluations picked up the stellar parameters effectively, and we estimate, with equivalently $\Delta\chi^2 = 1$, the errors to be $\dot{M}_* = (2\pm0.5)\times10^{-5}M_\odot\,\mathrm{yr}^{-1}$, and $v_\infty = 1{,}300\pm100$ km s^{-1}. Note that, if we adopt a solar metallicity, as allowed by the abundance indicator $N2 \equiv$ [N II]λ6,583/H$_\alpha$, the best model will change to $R_* = 11.1R_\odot$, $M_* = 17.5M_\odot$, $L_* = 4.9\times10^5\,L_\odot$, $v_\infty = 1{,}700$ km s^{-1} and $\dot{M}_* = 2.4\times10^{-5}\,M_\odot\,\mathrm{yr}^{-1}$. This is consistent with the $0.4Z_\odot$ results within the errors except for a significantly higher terminal velocity.

The stellar parameters of this best model belong to a 'real' WN star from the stellar evolution tracks, with an effective temperature of 48 kK, an initial mass of $42M_\odot$, an age of about 5 Myr, and a remaining lifetime of about 0.3 Myr before it loses another $\sim6M_\odot$ and collapses into a black hole of $\sim12M_\odot$. This model is actually one of the best models derived from studies of the optical spectral energy distribution[8]. Comparing to the physical properties of Wolf-Rayet stars in the Milky Way[18], we find that T_*, L_*, $\dot{M}_*$ and v_∞ are consistent with those for a WN7/WN8 star. The absolute magnitude M_V for ULX-1 ($M_V = -5.9$ mag after extinction correction) is brighter by 0.5 mag, fully within the spread of absolute magnitudes for WN subtypes.

The mass of the Wolf-Rayet star can be more reliably estimated with the empirical mass–luminosity relation[17,18] as done for NGC 300 X-1[22]. In our case, $L_* = 5.4\times10^5L_\odot$, and this corresponds to a Wolf-Rayet mass of $19M_\odot$, quite consistent with the mass for the best model. The luminosity derived for solar metallicity will correspond to a Wolf-Rayet mass of $18M_\odot$. Hereafter we will use $19M_\odot$ for the Wolf-Rayet mass, with an estimated formal error of $1M_\odot$ to roughly reflect the difference between the model value and the empirical value. Given the stellar mass and radius of $10.7R_\odot$, we can obtain the orbital period[43] from its mean density ρ as $P = \sqrt{\rho/100}$ h ≈ 72 h if the Wolf-Rayet star is filling its Roche lobe. The true orbital period will be longer than 72 h if the Wolf-Rayet star is only filling part of its Roche lobe.

Searching for orbital periodicity. The radial velocity changes between 210 km s^{-1} and 330 km s^{-1} as measured by the He II 4,686 Å emission line should reflect the orbital motion of the Wolf-Rayet star. Although a broad He II 4,686 Å emission line can be produced from the X-ray heated accretion disk in some ULXs with rather high X-ray luminosities (for example, in NGC 1313 X-2 with $\sim10^{40}$ erg s^{-1}; ref. 14), this should not be the case for M 101 ULX-1 because its X-ray luminosities during the Gemini/GMOS observations were three orders of magnitude lower, and the disk heating effects are insignificant even in its outburst, based on the optical studies[8]. In addition, the line ratios for the heated accretion disk are different from the line ratios for the Wolf-Rayet star because the emission line forming regions and temperature structures are quite different, yet the observed line ratios can be well reproduced by the Wolf-Rayet star.

In order to search for the orbital periodicity, we assume a circular orbit and fit a sine curve $v_r = v_0 + K\sin[2\pi(t-t_1)/P + \varphi]$ to nine barycentre-corrected radial velocities; the radial velocity for March 17 was dropped from the analysis because the spectrum had a very low signal-to-noise ratio. The four parameters are the radial velocity of the binary mass centre v_0, the radial velocity semi-amplitude K, the orbital period P, and phase φ at the first observation. The search is carried out by minimizing χ^2 defined as $\chi^2 = \sum_{i=1}^{10}[v_r(t_i) - v_{r,i}]^2/\sigma_{v,i}^2$. The radial velocity errors $\sigma_{vr,i}$ are taken as the wavelength calibration error of 0.25 Å, or 15 km s^{-1}. The five radial velocity measurements from 13 May to 19 May suggest a period no longer than 10 days (Fig. 2). The 'amoeba' technique is used for χ^2 minimization, using initial guesses taken from the parameter grids with P from 3 to 10 days in steps of 0.01 days, K from 20 to 150 km s^{-1} in steps of 5 km s^{-1}, and φ from 0° to 360° in steps of 10°. The best solution is found at the minimum $\chi^2 = 1.6$, for which the best period $P = 8.24\pm0.1$ days and the best radial velocity semi-amplitude $K = 61\pm5$ km s^{-1}, with the 68.3% error determined with $\Delta\chi^2 = 1$. The fact that the radial velocity curve can be fitted with a sine curve suggests that the orbital eccentricity is small.

Given P and K, the mass function for M 101 ULX-1 can be computed as $f(M_*,M_\bullet,i) = \frac{PK^3}{2\pi G} = \frac{M_*^3}{(M_*+M_\bullet)^2}\sin^3 i = 0.178M_\odot$. This sets an absolute lower limit for the mass of the primary. In the case of ULX-1, more information can be extracted because we already know $M_* = 19M_\odot$. Given the equation $\frac{M_*^3}{(M_*+M_\bullet)^2}\sin^3 i = 0.178M_\odot$, the primary mass will increase monotonically when the inclination angle decreases, that is, changing from edge-on ($i = 90°$) towards face-on ($i = 0°$). Thus the minimum mass for the primary can be obtained when $i = 90°$, which is $M_\bullet = 4.6M_\odot$ after solving the equation $\frac{M_\bullet^3}{(M_*+M_\bullet)^2}\sin^3 i = 0.178M_\odot$. The minimum mass will be $M_\bullet = 4.4M_\odot$ if we use $M_* = 17.5M_\odot$. Such a compact primary can only be a black hole. This is thus the dynamical evidence for a black hole in a ULX.

Determining the properties of the Wolf-Rayet/black-hole binary. This section duplicates some text from the main article, but with additional technical details.

M 101 ULX-1 is thus a Wolf-Rayet/black-hole binary, only the third discovered so far after IC 10 X-1 and NGC300 X-1. The binary separation can be computed with Kepler's law $a^3 = \frac{G(M_*+M_\bullet)}{4\pi^2}P^2$, which increases monotonically for increasing black-hole mass, starting from $a = 50R_\odot$ for $M_\bullet = 4.6M_\odot$ to $a = 75R_\odot$ for $M_\bullet = 60M_\odot$ (Extended Data Fig. 3). The Roche lobe size for the secondary can be computed with $R_{cr} = af(q) = a0.49q^{2/3}/[0.6q^{2/3} + \ln(1+q^{1/3})]$ with $q = M_*/M_\bullet$, and the Roche lobe size for the black hole can be computed with the same formula but with different $q = M_\bullet/M_*$. As shown in Extended Data Fig. 3, the Roche lobe size for the black hole increases with the increasing black-hole mass, but the Roche lobe size for the secondary does not change much, from $R_{\mathrm{cr},*} = 25R_\odot$ for $M_\bullet = 4.6M_\odot$ to $R_{\mathrm{cr},*} = 23R_\odot$ for $M_\bullet = 10M_\odot$, and to $R_{\mathrm{cr},*} = 22R_\odot$ for $M_\bullet = 20M_\odot$.

Regardless of the black-hole mass, the secondary is filling only half of its Roche lobe by radius, and the black hole must be accreting from the Wolf-Rayet star winds. Because the black hole is at least $50R_\odot$ away from the Wolf-Rayet star, the stellar wind must have reached close to its terminal velocity. The capture radius for the wind accretion can be computed as $r_{\mathrm{acc}} = \frac{2GM_\bullet}{v_\infty^2}$ and the accretion rate can be computed as $\dot{M}_\bullet = \frac{\pi r_{\mathrm{acc}}^2}{4\pi a^2}\dot{M}_*$. Given that the average luminosity for M 101 ULX-1 is about 3×10^{38} erg s^{-1}, the required accretion rate is $\dot{M}_\bullet = L\Big/\eta c^2 \approx \frac{L_{38}}{\eta}2\times10^{-9}M_\odot\,\mathrm{yr}^{-1} = \frac{1}{\eta}6\times10^{-9}M_\odot\,\mathrm{yr}^{-1}$. To capture this much stellar wind matter, as shown in Extended Data Fig. 4, the black-hole mass must be greater than $46M_\odot$ for $\eta = 0.06$ in the case of a non-spinning Schwarzschild black hole, and greater than $13M_\odot$ for $\eta = 0.42$ in the case of a maximally spinning Kerr black hole. If we use the velocity law $v(r) = v_\infty(1 - R_*/r)\beta$ with $\beta = 1$ for the inner wind[16], then the black-hole mass must be greater than $28M_\odot$ for $\eta = 0.06$ in the case of a non-spinning Schwarzschild black hole, and greater than $8M_\odot$ for $\eta = 0.42$ in the case of a maximally spinning Kerr black hole. If we adopt a typical η value of 0.1, the required accretion rate corresponds to $M_\bullet > 24M_\odot$ (and $i < 17°$) for a wind velocity of $v \approx 1{,}100$ km s^{-1}, and corresponds to $M_\bullet > 32M_\odot$ (and $i < 14°$) for the terminal velocity. The accretion rate argument thus requires a black hole of $>8M_\odot$–$46M_\odot$, likely to be a black hole of $20M_\odot$–$30M_\odot$ similar to IC 10 X-1 and NGC 300 X-1.

The recurring X-ray/optical outbursts dictate the presence of an accretion disk prone to instability, and the disk formation under stellar wind accretion places stringent constraints on the binary system. To explore why the number of Galactic X-ray stars is so small, it has been shown[44] that in the case of accretion of stellar wind matter in a detached binary system the specific angular momentum of the matter captured by the compact object is typically small. Therefore, usually no accretion disk is formed around the compact object. Consequently, very special conditions are required for a black hole in a detached binary system to be a strong X-ray source. A disk may form if the specific angular momentum of accreting matter, $Q_{\mathrm{acc}} = \frac{1}{4}\frac{2\pi}{P}r_{\mathrm{acc}}^2$, exceeds the specific angular momentum of the particle at the innermost stable circular orbit, $Q_{\mathrm{ISCO}} = \sqrt{3}r_g c = \sqrt{3}\frac{2GM_\bullet}{c^2}c$. This is usually expressed as $P < 4.8\frac{M_\bullet/M_\odot}{v_{1000}^4}\delta^2$ h, where $\delta \approx 1$ is a dimensionless parameter[19,45]. Given $P = 8.24\pm0.1$ days and $v_\infty = 1{,}300\pm100$ km s^{-1} for M 101 ULX-1, the black-hole mass is required to be $M_\bullet > 80M_\odot$, corresponding to $i = 9°$ (that is, nearly face-on). If the wind velocity from the velocity model of the inner wind[16] is adopted, then the black-hole mass is required to be $M_\bullet > 48M_\odot$, corresponding to $i = 11°$.

To investigate the possible presence of a partial ionization zone, we need to compute the temperature structure $T_d(r)$ for the accretion disk, especially for the outer disk. Following the procedures designed for an X-ray irradiated black-hole binary model for ULXs[46], we compute the disk temperature structure for a standard accretion disk with the α prescription[47] plus X-ray irradiation[43]. As shown in Extended Data Fig. 5, regardless of the black-hole mass for M 101 ULX-1, its outer disk temperature is as low as 4,000 K in the low-hard state owing to its large separation and large disk, and the helium partial ionization zone at about 15,000 K is bound to exist unless the black-hole mass is lower than $5.5M_{\odot}$. In comparison, the disk temperature for NGC 300 X-1, with an orbital period of 32.8 h and its WN5 star ($M_* = 26M_{\odot}$, $R_* = 7.2R_{\odot}$) filling its Roche lobe[22], never drops below 20,000 K owing to its small separation and small disk, and there is no helium partial ionization zone in the disk. This explains naturally why NGC 300 X-1 and similarly IC 10 X-1 exhibit steady X-ray radiation despite the apparent variations due to orbital modulation under the edge-on viewing geometry.

The existence of an accretion disk in M 101 ULX-1 is also supported by the observed spectral state changes, which resemble those for Galactic black-hole binaries[9,11] that are believed to reflect changes in the properties of their accretion disks[10]. During its outbursts, M 101 ULX-1 exhibits an X-ray spectrum[4,7] that can be classified as a thermal dominant state (albeit with exceptionally low disk temperatures), a well-defined spectral state that corresponds to a standard thin accretion disk at about 10% of its Eddington luminosity. Quantitative studies[23] show that when the luminosity exceeds 30% of the Eddington limit, the emission changes such that the X-ray spectrum includes a steep power-law with a significant hard component above 2 keV. The presence of such a hard component is not seen in the X-ray spectra of M 101 ULX-1. Given its bolometric luminosity of 3×10^{39} erg s^{-1} in the thermal dominant state at less than 30% of its Eddington limit, we infer that the black-hole mass is above $80M_{\odot}$. If this is true, the inferred black-hole mass of M 101 ULX-1 may challenge the expectations of current black-hole formation theories. The most massive black holes that can be produced for solar metallicity are about $15M_{\odot}$, and about $20M_{\odot}$ ($25M_{\odot}$, $30M_{\odot}$) for $\times 0.6$ ($\times 0.4$, $\times 0.3$) solar metallicity owing to reduced stellar winds and hence reduced mass loss in the final stages before stellar collapse[48].

31. Freedman, W. *et al.* Final results from the Hubble Space Telescope key project to measure the Hubble Constant. *Astrophys. J.* **553,** 47–72 (2001).
32. Kong, A. K. H., Rupen, M. P., Sjouwerman, L. O. & Di Stefano, R. in *Proc. Papers 22nd Texas Symp. Relativistic Astrophys. Stanford* (eds Chen, P., Bloom, E., Madejski, G. & Patrosian, V.) 606–611 (Stanford Univ. Press, 2005).
33. Bresolin, F. The oxygen abundance in the inner H II regions of M101: implications for the calibration of strong-line metallicity indicators. *Astrophys. J.* **656,** 186–197 (2007).
34. Liu, J. F. Chandra ACIS survey of X-ray point sources in 383 nearby galaxies. I. The source catalog. *Astrophys. J.* **192** (suppl.), 10–64 (2011).
35. Kong, A. K. H. & Di Stefano, R. An unusual spectral state of an ultraluminous very soft X-ray source during outburst. *Astrophys. J.* **632,** L107–L110 (2005).
36. Kuntz, K. D. *et al.* The optical counterpart of M101 ULX-1. *Astrophys. J.* **620,** L31–L34 (2005).
37. Pettini, M. & Pagel, B. E. J. [OIII]/[NII] as an abundance indicator at high redshift. *Mon. Not. R. Astron. Soc.* **348,** L59–L63 (2004).
38. Osterbrock, D. *Astrophysics of Gaseous Nebulae and Active Galactic Nuclei* (University Science Books, 1989).
39. Hamann, W. R., Koesterke, L. & Wessolowski, U. Spectra analysis of the Galactic Wolf-Rayet stars — a comprehensive study of the WN class. *Astron. Astrophys.* **274,** 397–414 (1993).
40. Crowther, P. A. & Hadfield, L. J. Reduced Wolf-Rayet line luminosities at low metallicity. *Astron. Astrophys.* **449,** 711–722 (2006).
41. Smith, L. F., Shara, M. M. & Moffat, A. F. J. A three-dimensional classification for WN stars. *Mon. Not. R. Astron. Soc.* **281,** 163–191 (1996).
42. Girardi, L. *et al.* Theoretical isochrones in several photometric systems. I. Johnson-Cousins-Glass, HST/WFPC2, HST/NICMOS, Washington, and ESO imaging survey filter sets. *Astron. Astrophys.* **391,** 195–212 (2002).
43. Frank, J., King, A. & Raine, D. *Accretion Power in Astrophysics* (Cambridge Univ. Press, 2002).
44. Illarionov, A. F. & Sunyaev, R. A. Why the number of Galactic X-ray stars is so small? *Astron. Astrophys.* **39,** 185–195 (1975).
45. Ergma, E. & Yungelson, L. R. CYG X-3: can the compact object be a black hole? *Astron. Astrophys.* **333,** 151–158 (1998).
46. Liu, J. F., Orosz, J. & Bregman, J. N. Dynamical mass constraints on the ultraluminous X-ray source NGC 1313 X-2. *Astrophys. J.* **745,** 89–110 (2012).
47. Shakura, N. I. & Sunyaev, R. A. Black holes in binary systems. Observational appearance. *Astron. Astrophys.* **24,** 337–355 (1973).
48. Belczynski, K. *et al.* On the maximum mass of stellar black holes. *Astrophys. J.* **714,** 1217–1226 (2010).

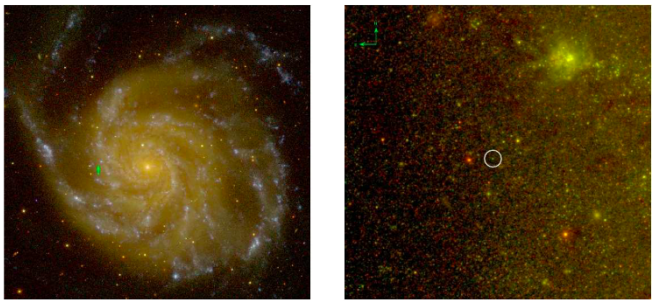

Extended Data Figure 1 | M 101 ULX-1 as observed in the optical region. Left, M 101 ULX-1 is located on a spiral arm of the face-on grand-design spiral galaxy M 101, as indicated by the arrow. The colour image of M 101 is composed of GALEX NUV, SDSS g, and 2MASS J images. Right, ULX-1 is identified as a blue object with $V = 23.5$ mag at the centre of the 1″ circle on the HST image. The colour image is composed of ACS/WFC F435W, F555W and F814W images.

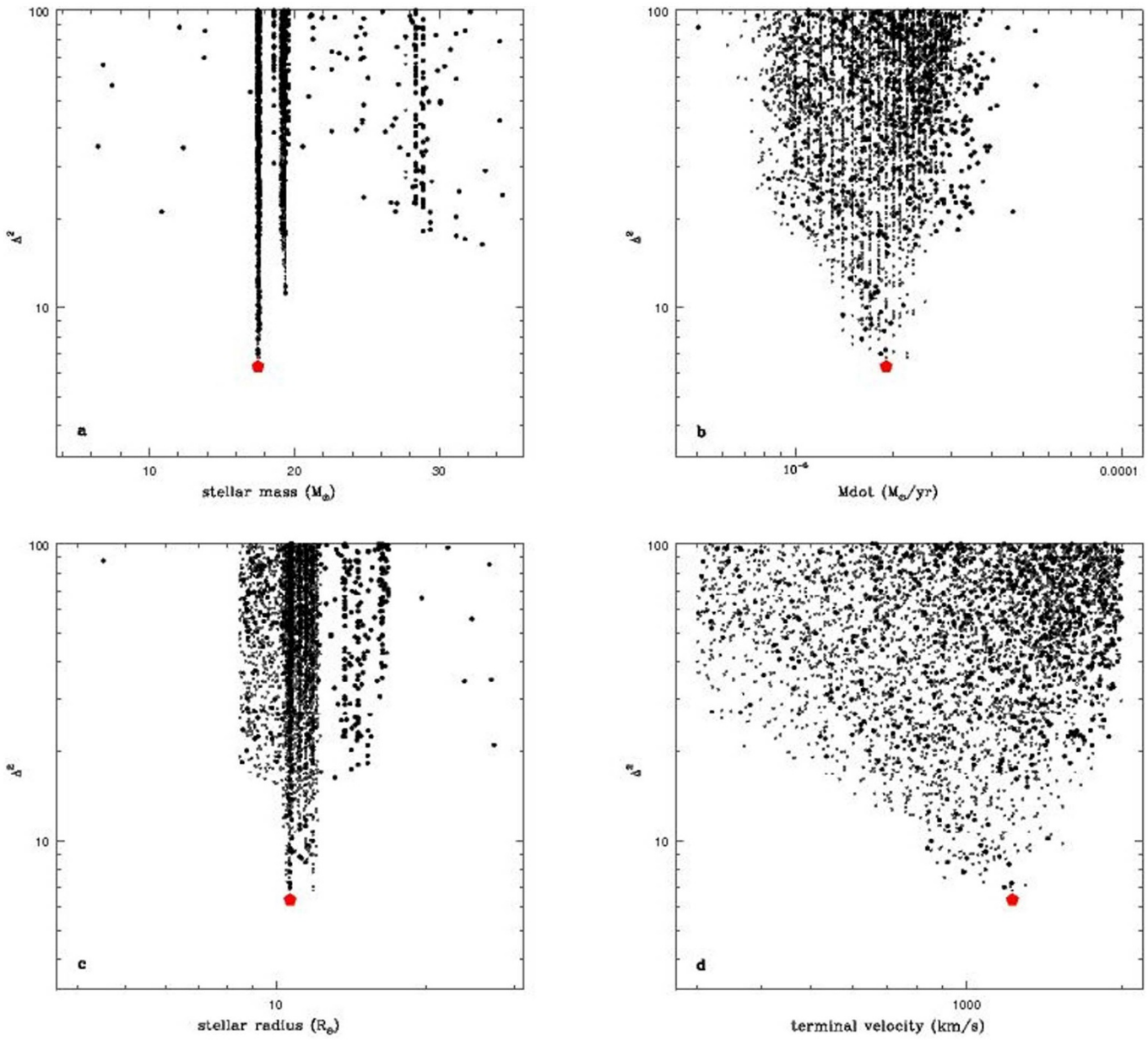

Extended Data Figure 2 | Physical properties of the Wolf-Rayet secondary from spectral line modelling. Distributions of computed Δ^2 as a function of stellar masses (**a**), stellar mass loss rate (**b**), stellar radii (**c**) and terminal velocity (**d**). Here $\Delta^2 = \Sigma_i(\mathrm{EW} - \mathrm{EW}_i)^2$ computes the difference between observed and synthetic equivalent widths EW for six broad helium lines present in the Gemini/GMOS spectrum. We have computed synthetic spectra for a group of 5,000 real stars from the evolution tracks (as shown by the thick stripes in the mass plot and the radius plot) and for another group of 'fake' stars with continuous distributions in mass, radius and luminosity. The best model is labelled by a filled pentagon in all panels.

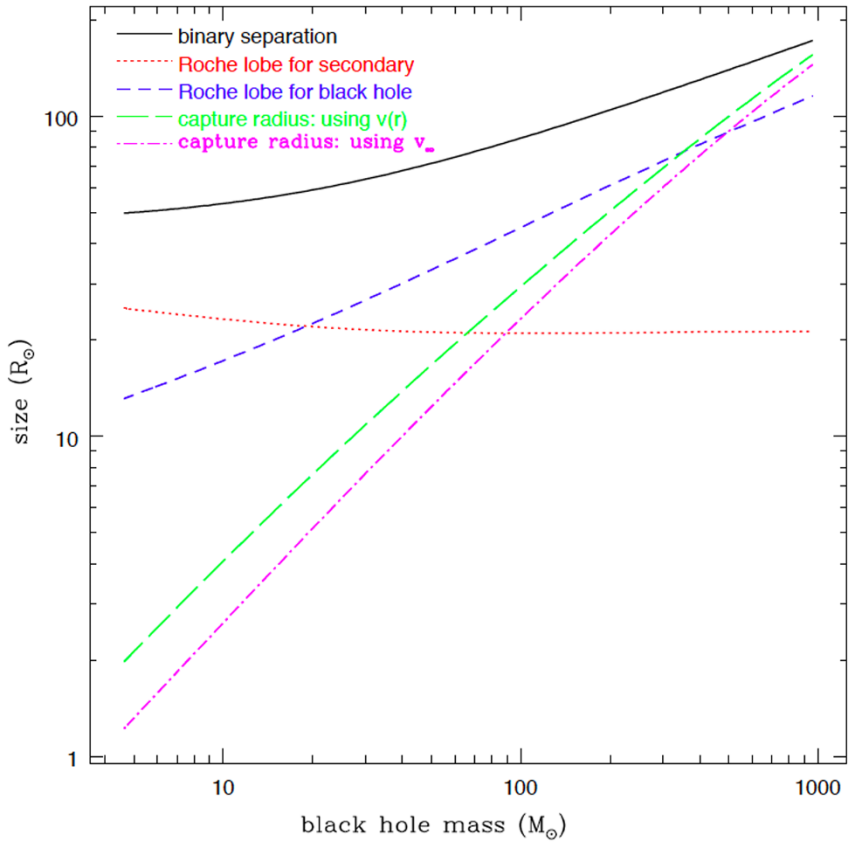

Extended Data Figure 3 | Properties of the Wolf-Rayet/black-hole binary for different black-hole masses. Shown are the binary separation (solid line), the Roche lobe sizes for the Wolf-Rayet star (dotted) and for the black hole (short dashed), the capture radius for the black hole when using the terminal velocity (dash–dotted) or when using a simplified velocity law $v(r) = v_\infty(1 - R_*/r)$ (long dashed).

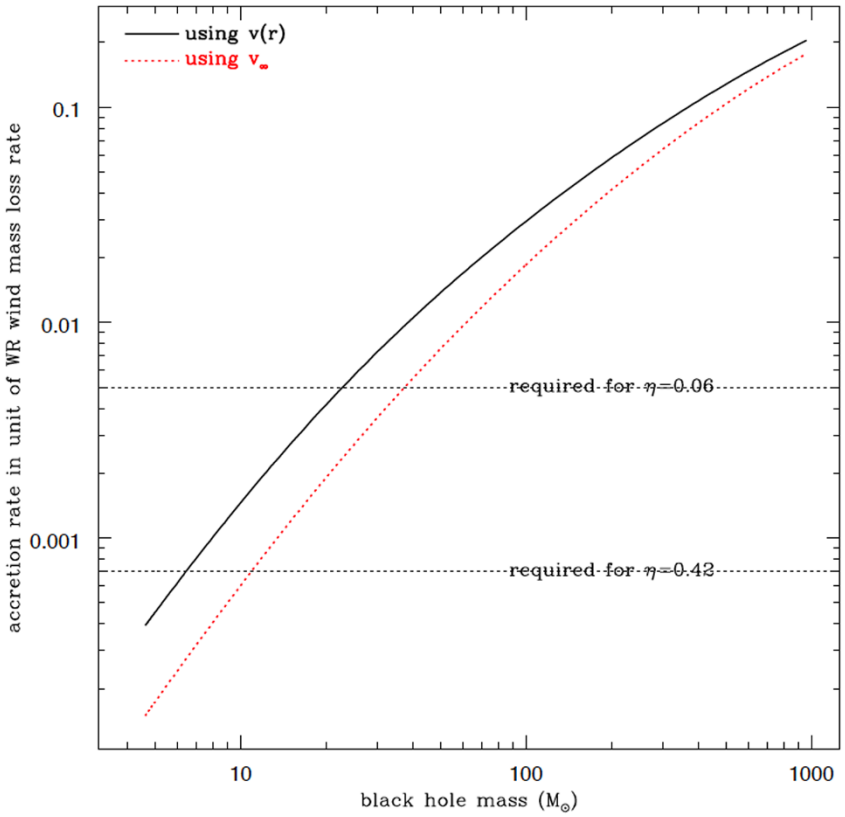

Extended Data Figure 4 | The black-hole accretion rate for different black-hole masses. The accretion rates are computed adopting the terminal velocity (dotted) and a simplified velocity law $v(r) = v_\infty(1 - R_*/r)$ (solid). To power the observed average luminosity of 3×10^{38} erg s^{-1}, the black-hole mass must exceed $13M_\odot$ ($8M_\odot$) using the terminal velocity (the velocity law) for a Kerr black hole ($\eta = 0.42$), and exceed $46M_\odot$ ($28M_\odot$) for a Schwarzschild black hole ($\eta = 0.06$). The two horizontal dotted lines indicate the accretion rates required for $\eta = 0.06$ and $\eta = 0.42$, respectively.

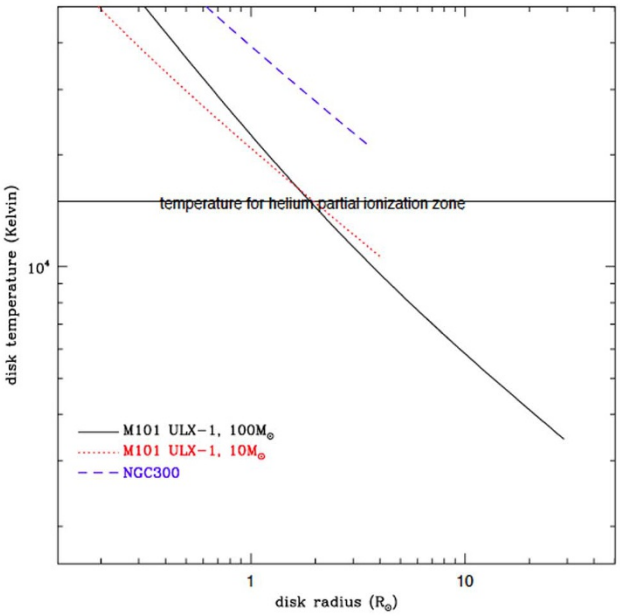

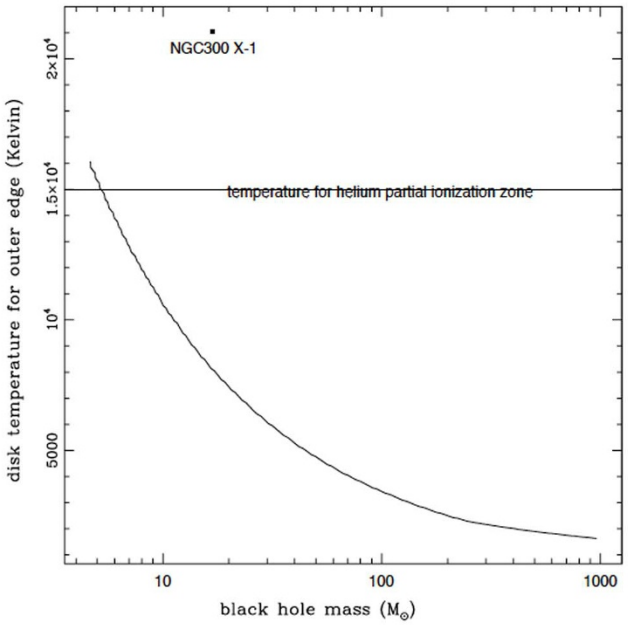

Extended Data Figure 5 | Disk temperature structures for M 101 ULX-1. **a**, The disk temperature profiles for M 101 ULX-1 (for $P = 8.24$ days, $M_* = 19M_\odot$, $R_* = 10.7R_\odot$, $M_\bullet = 10M_\odot$ or $100M_\odot$) and NGC300 X-1 (for $P = 32.4$ h $M_* = 26M_\odot$, $R_* = 7.2R_\odot$, $M_\bullet = 16.9M_\odot$; ref 22). **b**, The disk temperature at the outer edge for different black-hole mass in M 101 ULX-1. The horizontal line indicates the temperature required for the helium partial ionization zone.

Extended Data Table 1 | Gemini/GMOS spectroscopic observations of M 101 ULX-1

OBSDATE	MJD	exposure (second)	bary. (km/s)	velocity (km)
2010-02-15	55242.58343	3200	7.4	212
2010-02-16	55243.50615	3200	7.3	236
2010-03-16	55271.54390	3200	0.1	301
2010-03-17	55272.54564	3200	-0.2	—
2010-04-17	55303.47547	4800	-7.7	326
2010-05-13	55329.33126	6400	-12.2	302
2010-05-14	55330.39682	6400	-12.4	256
2010-05-15	55331.37803	6400	-12.5	227
2010-05-18	55334.41410	9600	-13.0	244
2010-05-19	55335.42391	9600	-13.1	305

The columns are: (1) observation date, (2) modified Julian date, (3) exposure time in seconds, (4) barycentric correction computed with rvsao, and (5) the corrected radial velocity as measured with He II 4,686 Å, with an error of 15 km s^{-1} as mainly from the uncertainties in the wavelength calibration.

Extended Data Table 2 | Properties of emission lines

Line ID	FWHM (Å)	E.W. (Å)	Lum. 10^{34}erg/s	model (Å)
HeII 4686	19.3	21.83 ± 0.20	43	21.75
HeI 5876	19.0	34.78 ± 0.29	49	34.21
HeI 6679	18.8	25.74 ± 0.37	24	26.56
HeII 5411	20.5	5.46 ± 0.13	8.3	6.10
HeI 4922	13.4	5.80 ± 0.64	8.4	3.91
HeI 4471	12.1	3.86 ± 0.65	7.0	5.18
H_γ	3.6	1.35 ± 0.22	2.7	
H_β	4.5	7.51 ± 0.06	12	
H_α	4.7	26.54 ± 0.46	34	
$[OIII]$ 4960	4.4	23.70 ± 0.49	40	
$[NII]$ 6548	3.8	3.85 ± 0.39	4.7	
$[NII]$ 6583	4.7	16.66 ± 0.08	18	
$[SII]$ 6716	4.0	4.58 ± 0.07	4.0	
$[SII]$ 6731	4.6	3.81 ± 0.06	3.1	

The columns are: (1) emission line ID, (2) FWHM as obtained from Gaussian fit, which equals 2.35σ, (3) equivalent width, (4) line luminosity in units of 10^{34} erg s^{-1}, and (5) equivalent width from the best Wolf-Rayet synthetic model.